Ultrasound in Med. & Biol., Vol. 36, No. 7, pp. 1135–1144, 2010

0301-5629/$–see front matter

ELSEVIER

doi:10.1016/j.ultrasmedbio.2010.04.017

● *Original Contribution*

DEVELOPMENT OF A RANGE OF ANATOMICALLY REALISTIC RENAL ARTERY FLOW PHANTOMS

Deirdre M. King,* Michael Ring,† Carmel M. Moran,‡ and Jacinta E. Browne*

*Medical Ultrasound Physics and Technology Group, School of Physics, Dublin, Ireland; †School of Manufacturing & Design, Dublin Institute of Technology, Dublin, Ireland; and ‡Department of Medical Physics, University of Edinburgh, Edinburgh, UK

(*Received* 22 *September* 2009; *revised* 18 *April* 2010; *in final form* 29 *April* 2010)

Abstract—Computer-aided modelling techniques were used to generate a range of anatomically realistic phantoms of the renal artery from medical images of a 64-slice CT data set acquired from a healthy volunteer. From these data, models of a normal healthy renal artery and diseased renal arteries with 30%, 50%, 70% and 85% stenoses were generated. Investment casting techniques and a low melting point alloy were used to create the vessels with varying degrees of stenosis. The use of novel inserts significantly reduced the time, materials and cost required in the fabrication of these anatomically realistic phantoms. To prevent residual metal remaining in the final phantom lumens a technique employing clingfilm was used to remove all molten metal from the lumen. These novel flow phantoms developed using efficient methods for producing vessels with various degrees of stenosis can provide a means of evaluation of current and emerging ultrasound technology. (E-mail: king.deirdre@mayo.edu) © **2010 World Federation for Ultrasound in Medicine & Biology.**

Key Words: **Anatomical flow phantom, Renal arteries, Doppler ultrasound, Stenosis, Tissue mimicking material, *In vitro* experimentation.**

INTRODUCTION

Renal artery stenosis (RAS) is a blockage or narrowing of the major arteries that supply blood to the kidney. RAS is present in 1% to 5% of all cases of hypertension and increases to 16% to 32% in populations who show specific history and clinical signs supporting the suspicion of renovascular hypertension (Olin et al. 1995; Radermacher and Brunkhorst 1998). Renal artery stenosis is considered the most common cause of potentially curable renovascular hypertension. If left untreated this progressive disease has many associated morbidities including progressive renal insufficiency, myocardial infarction, congestive heart failure, stroke and death. The current gold standard for detecting RAS is digital subtraction angiography (DSA), however, it is an invasive and expensive procedure that carries the risk of complications such as bleeding, anaphylaxis and contrast induced nephropathy (Williams et al. 2007). The noninvasive medical diagnostic imaging techniques currently available are duplex ultrasound, computed tomography (CT) and magnetic resonance imaging (MRI).

Duplex ultrasound is the most utilized method for noninvasive imaging of the renal arteries as it is the most widely available equipment and is not as expensive as MRI or CT techniques (Staub et al. 2007). Duplex ultrasound combines the direct visualisation of the renal arteries and kidneys via B-mode imaging, with Doppler measurement of the velocity of blood flow in the main renal artery and within the kidney allowing both anatomical evaluation and hemodynamic assessment. Typically, the classification of RAS is based on the maximum velocity obtained in the region of the maximum velocity through the neck of the stenosis. This maximum velocity is used to classify the severity of the stenosis because, for a constant flow rate, a tighter constriction leads to higher velocities through the stenosis.

Limitations of ultrasound examinations include its dependence on operator skill, the diminished ability to visualise accessory renal arteries and the difficulty in imaging obese patients or patients with intervening bowel gas (Paven et al. 2006). In addition, it is known that linear and curvilinear transducers of clinical ultrasound systems overestimate maximum velocity when measured from the spectral waveform, because of geometric spectral

Address correspondence to: Deirdre M. King, PhD., Department of Radiology, Mayo Clinic, 200 First Street SW., Rochester, MN, 55905 USA. E-mail: king.deirdre@mayo.edu

broadening (Daigle et al. 1990; Hoskins 1991, 1996). There are other known sources of error, such as velocity-gradient spectral broadening and lack of knowledge of the true direction of motion due to the single-component nature of commercial Doppler systems. Therefore, errors in the maximum velocity measurements in the renal artery can lead to over estimation in the degree of stenosis measured. In general, arterial flows are complex and there is a need to assess the accuracy of such measurements in a phantom for which the velocity distribution is accurately known. With *in vitro* phantom experiments, the values of the flow parameters are established; hence, it is possible to obtain accurate flow measurements allowing an estimation of mimicked disease progression and to directly compare each imaging technique using one reference standard. Ultrasound flow phantoms are used to test both the accuracy of ultrasound scanners (maximum velocity estimation) under standardised conditions that can be reproduced in many locations and to contribute to the understanding of normal and diseased states in the vascular system (velocity profile of blood).

Many different types of flow phantoms have been developed and a full review of these phantoms may be found elsewhere (Hoskins 2008; IPEM 1994; Law et al. 1989). The simplest type of flow phantom consists of a straight tube (rubber or plastic) embedded in a tissue mimicking material (TMM) through which blood mimicking fluid (BMF) is pumped (Douville et al. 1983; Frayne et al. 1993; Law et al. 1989). This simple type of flow phantom lacks the complexity of human vessels, such as irregular lumens and the presence of stenosis. The most commonly employed vessel materials in such phantoms were commercially available tubing but such tubing had the incorrect acoustic properties to mimic human vessels (IPEM 1994).

Wall-less phantoms overcame these problems and allowed for more complicated geometries to be produced by using lost core casting techniques (Poepping et al. 2002; Smith et al. 1999). In an attempt to reproduce realistic physical replicas of human vasculature, excised vessels or vessels from cadavers have been used (Dabrowski et al. 1997, 2001). However, excised arteries are susceptible to geometric and acoustic changes if they are not stored properly (Wilhjelm et al. 1997). It is difficult to characterise excised vessels and especially to reproduce many copies of an exact specified geometry. In addition, the use of excised vessels requires strict attention to issues of biologic safety and to legislation regarding the use of excised human tissues. Therefore, it is desirable to use materials that can be well characterised and easily reproduced for *in vitro* testing.

To date the majority of work on anatomical flow phantoms has concentrated on the development of realistic carotid flow phantoms (Frayne et al. 1993; Meagher et al. 2007; Poepping et al. 2002, 2004; Smith et al. 1999; Watts et al. 2007). These anatomical flow phantoms have proved to be powerful research tools and have helped to improve the understanding of normal hemodynamic patterns and their correlation with the development of vascular stenosis at the bifurcation of the carotid artery. These *in vitro* experimentations along with clinical studies have helped Duplex ultrasound replace DSA as the technique most widely used to quantify stenosis grade in the carotid arteries and to select patients for subsequent tests, or surgical or medical therapy (Grant et al. 2003; Netuka et al. 2006).

Developments in computer-aided design (CAD) and rapid prototyping (RP) have allowed three-dimensional (3-D) anatomical reconstruction using data from clinical 3-D data sets obtained from high-resolution 3-D imaging techniques such as MRI and CT (Allard et al. 2009; O'Flynn et al. 2005; Renaudin et al. 1994; Watts et al. 2007; Yedavalli et al. 2001). The aim of this study was the construction and validation of reproducible renal artery flow phantoms designed with the vessel depth and orientation similar to that found *in vivo*.

MATERIALS AND METHODS

General study design

To develop an anatomically realistic renal artery flow phantom a number of vessels with similar geometries to that of the renal artery *in vivo* were constructed. This was achieved by obtaining a physical replica of the renal artery using computer aided design and rapid prototyping. This physical replica was then used to create a negative mould into which a low melting point alloy was poured. Using this metal core, it was possible to create a lumen in a tissue mimicking material that had similar geometries to a renal artery *in vivo*. The steps involved in creating this phantom are discussed in more detail in the following section.

Fabrication of the renal artery model

A 3-D computer model of the renal artery was developed using a 64-slice CT data set of the abdominal region acquired from a healthy volunteer (who gave informed consent) with normal renal vasculature (Fig. 1). Ethics approval was obtained from Dublin Institute of Technology's Research Ethics Committee. The data were obtained using a Siemens SOMATOM Sensation Cardiac 64 (Siemens Medical Solutions, Karlsruhe, Germany), 64 images (slices) per rotation at 0.7 mm resolution. The CT images were imported into a commercial software package (MIMICS 10, Materialise, Leuven, Belgium) which provided an interface for the visualisation and segmentation of CT images and the 3-D rendering of a region-of-interest (ROI). Using MIMICS the

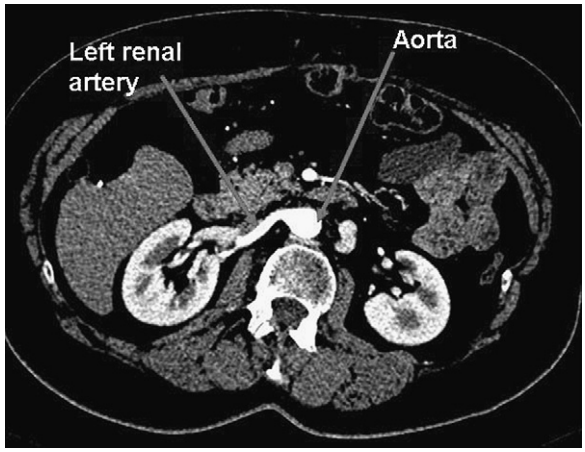

Fig. 1. A computed tomography (CT) slice (Siemens SOMATOM Sensation Cardiac 64) of the abdominal region from a healthy volunteer with the aorta and left renal artery highlighted.

two-dimensional (2-D) scan slices were viewed and the area including the left renal artery and aorta was selected in each slice by the author. The left renal artery was chosen as it was clearly identifiable in the CT images having a more horizontal and straight course. A mask was created to select the portions of the scan that were relevant to the studies and a threshold was applied to the grey-scale images ensuring that only the pixels corresponding to the tissues of the correct density were highlighted (renal artery and aorta). Each slice was inspected and edited by the author if extra surrounding soft tissue with a similar density had also been highlighted. From the defined ROI a 3-D computer model was rendered.

The resulting computer model was exported as a STL file into the 3-D CAD design software program SolidWorks® (Dassault Systèmes SolidWorks Corp., Concord, MA, USA) where the model was further refined to produce a generic model of the renal artery as follows. A spline curve was created which followed the axis of the vessel lumen reconstruction projected in one plane. The spline curve was adjusted in the other two orientations to account for out-of-plane curvature of the vessel lumen. The solid sweep command was used to construct the renal artery with a 6.8 mm diameter along the whole length of the model that followed the path of the spline. To aid centering of the renal artery metal core in the silicone master mould, an extrusion was constructed at each end of the model. These extrusions were 10 mm (in length) four-sided projections on each end of the renal artery model (Fig. 2).

To develop diseased renal artery computer models an experienced vascular clinical measurement scientist was consulted and a series of hand drawings highlighting the position and extent of RAS with various degrees of blockage were prepared. The position of the blockage

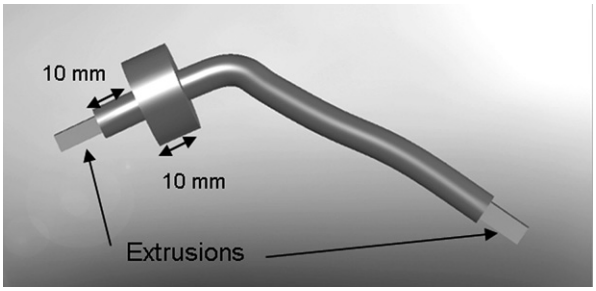

Fig. 2. Normal renal artery computer model with 10 mm extrusions and modified section of blockage insert.

was chosen at approximately 10 mm from one end of the model as it has been shown that up to 66% of RAS is due to atherosclerosis, which typically involves the ostium and proximal 20 mm of the renal artery (Beattie et al. 1997). Originally in the computer model of the diseased renal arteries, the chosen area for the blockage was scaled about its centroid by an amount that corresponded to the desired degree of stenosis. While designing the 70% and 85% diseased models it was believed that this method would produce models so fragile that they would break during rapid prototyping. To overcome this problem a type of ''goalpost support'' was used. These supports were built on the top and bottom of the stenosis to frame the area and provide extra support while the model was being machined. Unfortunately, even with the presence of the supports, the stenosis area was still too weak and fragile.

An alternative method was developed, instead of producing a whole model for each diseased renal artery an insert with the desired blockage was rapid prototyped. The computer model of the normal renal artery was altered to accommodate these inserts. At the desired location of the blockage the diameter was increased from 6.8 mm to 20 mm, (Fig. 2). The computer model was split in half along the length of the model to aid the production of the negative master silicone mould.

Rapid prototyping (RP) is a type of computer aided manufacturing. The computer model of the renal artery was exported from SOLID WORKS into the RP machine in the form of STL files. The RP machine used was a Z printer 310 Plus 3-D printer (Zcorporation, Burlington, MA, USA). This used data from the STL file to produce a physical replica of the renal artery using a composite powder (ZP 131; Zcorporation) and a water-based resin. The slice thickness was 0.1 mm. It was important to choose a small slice thickness to minimise stepping effects and reduce the amount of manual finishing required. The RP model was carefully sanded to remove any ridges and the excess powder was vacuumed off. A cyanoacrylate adhesive (Z-bond 101; Zcorporation) was painted on all surfaces to strengthen, cure and seal the RP model.

A master silicone negative mould of the renal artery RP model was produced using a vacuum casting process. For the normal renal artery RP model, the split lines were selected where the two halves joined. Sellotape® (Henkel, Düsseldorf, Germany) (thickness 0.04 mm) was attached along the line and hooks were attached to the model using Araldite™ adhesive (Huntsman Advanced Materials (UK) Ltd., Cambridge, UK). Since the RP model was produced in two halves the Sellotape® did not affect the shape of the model as it was placed between the two halves. The model was placed in a box (14 cm × 7 cm × 4 cm) and hooked onto supports and silicone (Essil 291; Axson Technologies UK, Suffolk, UK) was poured in. When set the master silicone mould was split along the predefined parting plane and the RP model removed producing a negative mould of the renal lumen.

To produce the diseased models of the renal artery, a series of symmetrical stenoses inserts (30%, 50%, 70% and 90%), each 10 mm in length were developed in SolidWorks®. Each stenosis insert was modelled so that its surfaces were tangential to the surfaces of the renal artery at the edges of the stenosis. This procedure was repeated to generate a series of geometrically similar inserts that differed only in the reduction in diameter, the stenosis itself having been scaled in cross-section throughout. The inserts were rapid prototyped using the same method as descried for the renal RP model. The inserts were produced in two halves to allow easy removal of the inserts from the metal replicas (Fig. 3). The advantage of this method was that the outside walls of the inserts were thickened to increase the stability of the RP model even for 85% stenosis. In addition, it reduced the number of rapid prototyped models and silicone moulds required.

A low melting point alloy with a melting point of 47°C (MCP 47 Mining and Chemical Products Ltd., Northamptonshire, UK) was used to construct the renal artery metal core. The desired inserts were selected and slotted into the master silicone mould, which was clamped together using bar clamps applying equal pressure across the whole surface of the mould (ensuring the shape of the model was not changed) and sealed. The alloy was melted by heating it above 47°C and slowly poured into the fill port of the mould. When the alloy was set, it was removed from the mould, the inserts were removed and the metal core was hand polished. Suitable protective clothing (face mask, safety glasses, gloves and laboratory coat) were worn and extreme care was taken during polishing and filing because the alloy contains heavy metals such as lead and cadmium. This work should be performed in a fume hood to avoid the formation or spread of airborne dust as there is a danger to health by prolonged exposure through inhalation and skin contact. The renal artery metal cores produced are presented in Figure 4.

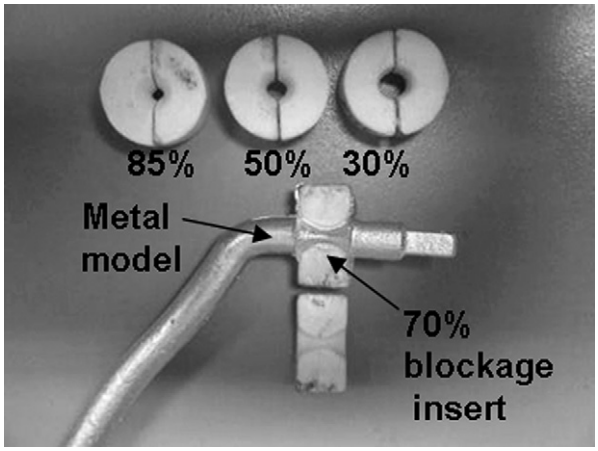

Fig. 3. The removable stenosis inserts used to cast the diseased metal cores of the renal artery.

Phantom construction

The phantom container's dimensions were 230.0 mm × 135.4 mm × 103.7 mm (L × W × H) with a wall thickness of 2.6 mm. In the phantom container, two plastic barbed connecters were modified to give a 7.5 mm i.d. (product number 06360-90; Cole-Parmer, Walden, UK) were secured to act as inlet and outlet ports. Nalgene® PVC plastic tubing 7.9 mm i.d. (product number 228-0607; VWR International, Dublin, Ireland) was attached to the connectors to allow the metal core to be secured between them. Reticulated foam (30 pores per inch, Foam Techniques, Northamptonshire, UK) (50 mm × 50 mm × 10 mm) was fixed using Araldite™ adhesive around the sides of the phantom container, the connectors and tubing to help seal the phantom (Ramnarine et al. 2001). Before securing the renal artery metal core in place, a single layer of clingfilm (thickness 0.1 mm) was

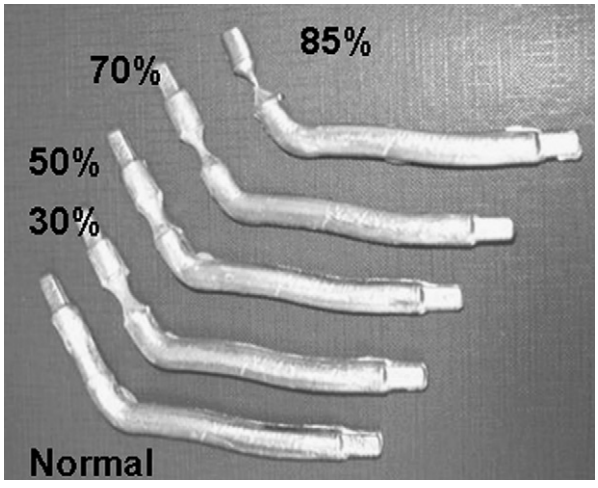

Fig. 4. Metal cores of the renal artery with varying degrees of stenosis (normal healthy artery, 30%, 50%, 70% and 85%) before polishing.

carefully wrapped around it. This was to overcome the problem of residual metal, which initially remained in the lumen (Figs. 5 and 6). At each end of the metal core, an extra length of clingfilm was passed out through the connectors. The renal artery metal core was secured between the two plastic tubes.

An agar-based TMM developed as part of the European Commission (EC) funded project was used (Teirlinck et al. 1998). Its composition and manufacture were as described in Ramnarine et al. (2001). This TMM is very well characterised and has good reproducibility and our results were found to agree with those of other groups (Brewin et al. 2008; Browne et al. 2003; Teirlinck et al. 1998). It has a reported speed of sound of 1541 ± 3 m s^{-1} and attenuation coefficient of 0.52 ± 0.03 dB cm^{-1} MHz^{-1} (Teirlinck et al. 1998). The TMM was allowed to cool to 42°C (stirring continuously) and then poured into the phantom container until 4.5 cm thickness of TMM covered the renal artery metal core, this is similar to the depth of renal arteries *in vivo*. When the TMM was set, the phantom was placed in a temperature controlled water bath (50°C ≤ T ≤ 60°C) for approximately 4 h to allow the renal artery metal core (melting point 47°C) to melt. No agar TMM was directly exposed to water in the bath as the phantom was sealed with a lid and the clingfim and metal core remained in the lumen until the phantom was removed from the bath. The clingfilm containing the molten metal was carefully removed resulting in a realistic renal artery lumen with no residual metal remaining.

To ensure long-term stability of the phantoms, when not in use they were stored in air-tight containers at room temperature with the scanning wells and lumens of the phantoms filled with a solution of 87.7% water, 11.8% glycerol and 0.5% Benzalkonium chloride (10%) similar to the water, glycerol and Benzalkonium chloride concentration in the TMM. This was to prevent the phantoms from (1) drying out, (2) bacterial growth and (3) prevent change in speed of sound due to loss of glycerol through diffusion.

Geometric accuracy

To ensure the fabrication method for the renal artery replica was reproducible, the geometric accuracy of the metal cores and corresponding phantom lumens was determined. The diameter of five metal cores was measured in three locations along their lengths to establish the statistical significance of any differences within and between the metal cores. The three locations measured were (1) 10 mm from inlet, (2) 10 mm from bend and (3) 10 mm from outlet, using vernier calipers. A one-way repeated measure of analysis of variance statistical test was carried out to compare diameters from the individual metal cores. This was repeated for the resultant

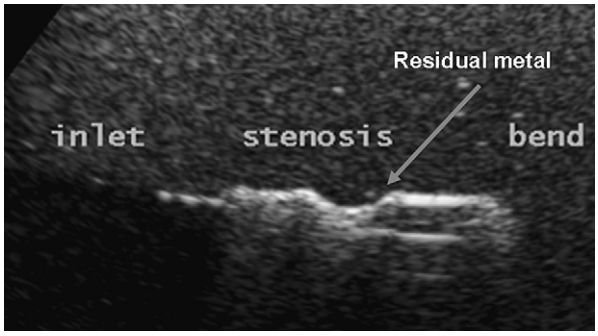

Fig. 5. B-mode image of 50% stenosis lumen with residual metal present.

vessel lumen diameters that were measured from B-mode transverse images acquired during test flow experimentation with the vessels filled with a speed of sound corrected solution (water 90.5%: glycerol 9.5% for an intended speed of sound of 1540 m s^{-1}) (Goldstein and Langrill 1979). Accurate relative positioning of the transducer was accomplished with a micromanipulator.

The vessel lumen diameter was determined by plotting the image intensity vs. distance across each region, as shown in Figure 7. Using MATLAB, a graphic interface displayed the intensity profile along a line of interest, allowing the user to specify the boundaries of the vessel. The peaks corresponding to the edges of the near and far walls were located. The distance in mm was calculated by measuring the known dimensions of the phantom (the thickness of the TMM was measured using acoustic speed of sound 1549 [± 5] m s^{-1} which had been measured using a scanning acoustic macroscope system which is described elsewhere (King 2009)) and converting the pixel distance measured (by the MATLAB program) into mm. The diameter of the vessel was then calculated using the maximum distance between the peaks. The difference in diameters between the original computer model, rapid prototype model, metal cores and vessel lumens were investigated using a repeated measure of analysis of variance statistical test. The null hypothesis being tested was that there was no difference in the dimensions of the models. If $p < 0.05$, the null hypothesis was rejected and there was a statistical difference in the dimensions of the models. All statistical tests were carried out using IBM SPSS Statistics™ 18 Statistical Software (SPSS Inc., Chicago, IL, USA).

Basic flow simulations

All phantoms were tested for leakage and examined for residual metal remaining in the lumen, since this could lead to imaging or flow artefacts. A HDI 3000 (ATL/Philips, Amsterdam, The Netherlands) with a linear broadband transducer (L12-5), was used to obtain

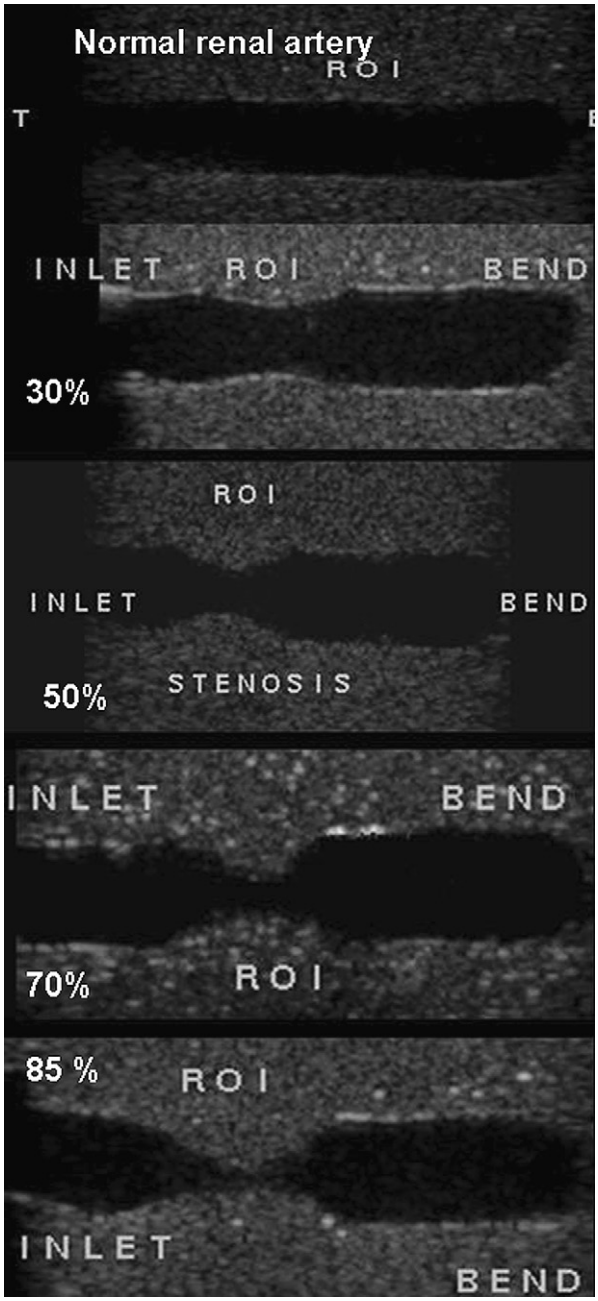

Fig. 6. B-mode images of wall-less phantom showing inlet of renal artery flow phantom with varying degrees of stenosis (normal healthy artery, 30%, 50%, 70% and 85%).

B-mode and colour Doppler images of each phantom. The phantoms were connected to a simple flow system, which provided *in vitro* flow. The BMF recommended in the IEC specifications was used and its composition (in % weight) is described by Ramnarine et al. (1998). The flow system consisted of a magnetically driven gear pump head (Cole Parmer, Walden, UK) coupled to a direct current servo motor (McLennan Servo Suppliers Ltd., Surrey, UK). The motor was driven by a servo amplifier (Aerotech Ltd., Berkshire, UK) and a computer controller program developed in Labview (National Instruments, Austin, TX, USA) was used to output a set mean velocity of 40 cm s^{-1} (calibrated using timed weight collection). BMF, which had been degassed using a sonicator, was pumped through the phantoms using the gear pump for 1 h prior to measurements to ensure no air bubbles remained.

RESULTS

Geometric accuracy

Using a one-way repeated measure of analysis of variance statistical test, no statistical difference in diameter measured in the metal cores ($p < 0.39$) or within the phantoms ($p < 0.09$). The mean diameters for each of the models (computer model, RP model, metal core and phantom lumen) are shown in Table 1. Note that the number of measurements for each model are as follows; RP is average from three measurements of one model, metal core mean is average of 15 measurements (three locations × five metal cores) and phantom lumen, mean is average of 15 measurements (three locations × five metal cores). The results of the one-way repeated measure of analysis show that the dimensions of the four models differ significantly $p < 0.05$. Post hoc tests revealed that the dimensions of the computer model were significantly different than RP model, metal core and phantom lumen ($p = 0.001$). The diameters of the RP model, metal core and phantom lumen were not significantly different from each other ($p > 0.05$). This difference in dimensions was as a result of the rapid prototyping process that resulted in the model diameter increasing by approximately 1 mm and the presence of the Sellotape® (0.04 mm thickness) for the creation of the split lines for the master silicone negative mould. Since this increase was found along the whole length of the model including the area of stenosis therefore the percentage of blockage remained the same, (the degree of stenosis was not affected).

The effect of clingfilm on the dimensions of the metal cores was also investigated, using a vernier calipers the diameter of the metal cores with and without the single layer of clingfilm were recorded along the length of the models and also at the stenosis region. It was found that it did not significantly alter the dimensions of the metal cores ($p < 0.05$). For each metal core, care was taken to ensure that the single layer of clingfilm did not have any creases that would transfer onto the TMM leaving the phantom lumen surface uneven.

Basic flow simulations

All phantoms developed underwent basic flow measurements for a minimum of 1 h to ensure there were no ruptures or leakage through the vessel lumen. There was no leakage of BMF through the normal healthy

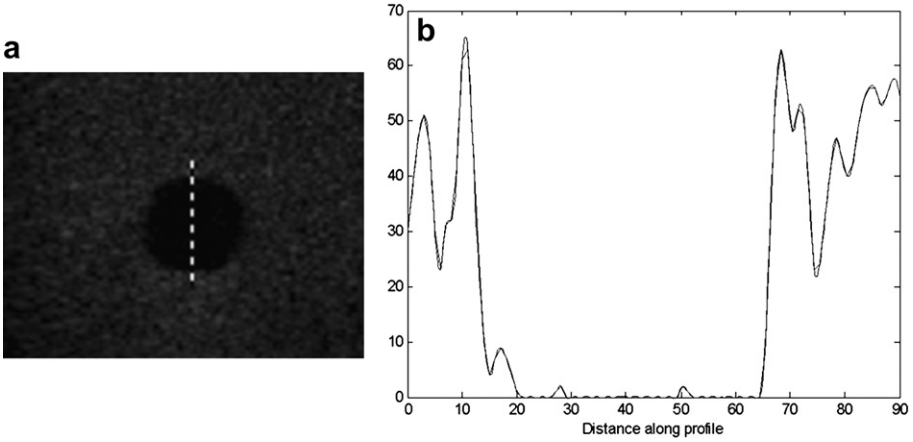

Fig. 7. Calculation of the vessel diameter from B-mode ultrasound image, (a) profile line marked across lumen and (b) plot of image intensity vs. distance along line of interest.

vessel, 30% and 50% stenosis lumens at a mean velocity of 40 cm s^{-1} after 5 h of continuous flow. The 70% phantom leaked 2 h after flow started at a velocity of 40 cm s^{-1}. The 85% phantom leaked within 1 h of starting flow. Presented in Figure 8 are images of the inlet region of the 30% and 70% wall-less phantoms. The colour Doppler image is of the inlet region of the renal artery with 70% stenosis, turbulent and reverse flow is evident in the post stenosis region (Fig. 8b).

The addition of Benzalkonium chloride (10%) to the water/glycerol solution, which was used in the scanning well and lumen of the phantoms during storage, successfully prevented any bacterial growth on the TMM over a period of 9 months. The acoustic properties of the TMMs were not tested over this period of time.

DISCUSSION

With the advancements in computer-aided design (CAD) and rapid prototyping, it is possible to produce flow phantoms with specific patient geometries. In this study, a realistic renal artery lumen similar to that found *in vivo* was constructed at a depth of 4.5 cm to mimic its location in the abdomen. The vessel was mounted in the horizontal plane, *in vivo* the renal arteries may be positioned at a variety of angles. It was decided for these initial phantoms to only use one vessel orientation for simplicity.

With the development of the novel stenosis inserts, it was possible to efficiently produce these phantoms at a reduced cost as only one master silicone negative mould was required to make the range of metal cores with increasing degrees of stenosis. Previous studies created a separate mould for each of the required blockages, which was time consuming and required several computer models, rapid prototyped models and silicone moulds (Poepping et al. 2002; Watts et al. 2007). These novel inserts also increased the stability of the metal core during the casting process even for the most stenosed models. By having the inserts in two halves, it allowed the easy removal of the metal core with out damaging the stenosis area. Extra care had to be taken for the 85% stenosis metal core as this was the most fragile model, in particular when mounting the core in phantom as to not to bend or break it at the point of stenosis. Also when pouring TMM, it was poured away from the area of the stenosis to prevent sagging at that point.

Although statistically significant differences were found between the original computer model and the final vessel lumen, these differences were due to the rapid prototyping process that resulted in the model diameter increasing by 1 mm. Once this difference in diameter is quantified and taken into account, it should be possible to create vessel lumens with precise accurate dimensions. As illustrated, there were no statistical differences between the metal cores and phantom lumens indicating that the fabrication methods were valid and reproducible. This allows for the fabrication and development of exact duplicates of the renal flow phantom to enable the study of disease progression in the renal artery with increasing stenosis. Meagher et al. (2007) also observed computer models which where significantly different in dimension to the metal cores. Although in this study there was a reduction in diameter, which was attributed to hand finishing and polishing of the metal cores.

Initially during the removal of the low melting point alloy from the phantom, a large amount of residual metal was found remaining in the lumen despite placing the phantoms in water bath ($50^{\circ}C \leq T \leq 60^{\circ}C$) for approximately 4 h and flushing water from the waterbath through the lumen. A number of studies have used similar low melting point alloys to create realistic vessels (Meagher et al. 2007; Poepping et al. 2002, 2004; Smith et al.

Table 1. The computer model, RP model, metal core and phantom lumen mean diameters ± 1.96 (Std. error) and corresponding 95% confidence intervals

Model	Mean (mm)	Std. error (mm)	N	95% Confidence interval	
				Lower	Upper
Computer	**6.8	0	1	6.8	6.8
RP	7.68	0.003	3	7.67	7.69
Metal core	7.64	0.013	15	7.61	7.67
Phantom lumen	7.67	0.016	15	7.64	7.70

N is the number of sample measurements.
** Denotes a statistical difference ($p < 0.05$) against the computer model and the RP, metal core and phantom lumen.

1999) and did not disclose any major problems with residual metal in phantoms. Smith et al. (1999) pumped nitric acid solution (7% NHO_3 by volume) through the phantom lumen for 4 h to ensure no residual metal was left. This was repeated in this study and, after 6 h, there was still a significant amount of low melting point alloy found remaining in the lumen particularly at the bend and at the site of stenosis by visually assessing US images of the lumen, Figure 5. This method was very time consuming and there was concern about the effect of the acid on the acoustic properties of the TMM as it was in constant contact within the TMM lumen. To overcome this problem a thin layer of clingfilm was wrapped around each of the metal cores before they were placed in the phantoms. Care was taken not to change the dimensions or geometry of the cores. This method was successful in removing all of the low melting point alloys, Figure 6. Recently Allard et al. (2009) suggested a new material as an alternative to low melting point alloys for the fabrication of realistic 3-D geometries. This new material Isomalt is a commercial sugar alcohol that totally dissolves in water at room temperature. This eliminates any residues and also the need to heat the phantom in a water bath which may result in leaching of glycerol and change in the properties of the TMM. In this study the presence of the clingfilm around the low melting point alloy gave extra protection to the TMM from leaching of glycerol from the TMM as the water was not in contact with the surface of the TMM. Further study is required for the use of Isomalt as a substitute for low melting point alloys as volume shrinkage was observed during cooling of the material.

Interestingly, the clingfilm also had an added advantage as it helped seal the TMM (while it was setting, after which it was removed containing the molten metal) around the inlet ports of the phantom. Wall-less flow phantoms have no tubing material and the BMF is in direct contact with the TMM. Therefore, it is important to have a good seal between the inlet and outlet tubes and the TMM vessel lumen to prevent BMF leakage. A number of methods have been described to seal the vessel adequately and overcome TMM rupture (Poepping et al. 2002; Ramnarine et al. 2001; Rickey et al. 1995). In the phantoms described here reticulated foam was placed around the connectors and tubing to help seal the phantom by aiding the adhesion between the TMM and wall of the container as described by Ramnarine et al. (2001). In early phantoms, before the metal cores were wrapped in clingfilm, BMF leakage occurred at the inlet due to splitting of the TMM. The problem was overcome by using the layer of clingfilm wrapped around the metal

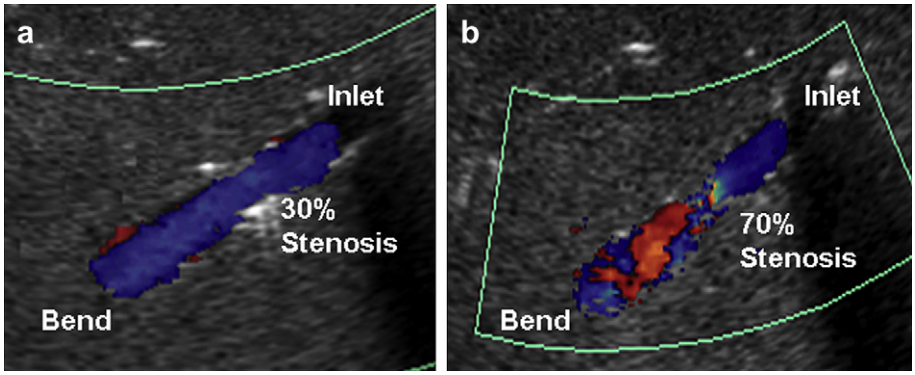

Fig. 8. Colour Doppler images showing (a) the inlet region of the vessel with 30% stenosis, a small area of reverse flow is present at the bend and (b) the inlet region of the vessel with 70% stenosis, turbulent and reverse flow are evident post stenosis.

core. The addition of the clingfilm helped seal the interface between the tubing and the TMM channel during the setting process. This resulted in a smooth continuous TMM surface once the metal core and clingfilm had been removed. Previously a ridge was present between the metal cores and the tubing providing a weak point where the TMM would split and rupture. The production of flow in such tight stenosis (70% and 85%) has been a challenge to a number of research groups, further refinement to prevent vessel rupturing is being investigated; one possible way of improving the design may be to increase the inlet length. These basic flow experiments have shown the potential for these anatomically realistic renal artery flow phantoms allowing interrogation along the entire vessel in a systematic manner and looking for changes in the maximum velocity related to known diameter reductions. Further flow experimentation using both steady and physiologic waveforms similar to that found in the renal artery has been performed by colleagues. These results will be presented in future publications.

A possible improvement to these phantoms would be the addition of a fat layer to replicate the *in vivo* situation. Fat layers are a major limitation in renal imaging as the presence of overlying subcutaneous fat layers in many patients gives rise to signal distortion and excessive attenuation of the ultrasound beam. Such an extension to the present work will likely produce clinically relevant results. By studying the effect of the fat mimicking layer using these realistic phantoms, a useful approximation to the errors in maximum velocity measurements may be determined and their implications for measurements in patients with RAS evaluated.

CONCLUSIONS

Using computer-aided modelling techniques reproducible renal artery flow phantoms with varying degrees of stenosis were constructed. For the fabrication of the diseased models, novel stenosis insert were designed which greatly reduced the time, materials and cost required for the development of these phantoms. The production of tight stenoses (70% and 85%) may require some refinement for flow experimentation to prevent vessel rupture. In common with other research groups such phantoms are difficult to manufacture and other possible techniques to increase their lifespan might be to alter the length of the vessel and these are a source of ongoing investigation. Currently, no anatomically realistic renal artery flow phantoms are available commercially. These novel renal phantoms developed and described in this work can provide a means of evaluating current and emerging ultrasound technologies in addition to being tools to observe the hemodynamic features within the renal artery.

Acknowledgments—The authors thank Sean Keane for technical assistance in the fabrication of the renal artery model. This work was supported by the Technological Sector Research Strand 1 Scheme, Higher Education Authority and the Research Support Unit of the Dublin Institute of Technology, grant TERS 2005. C. M. Moran would like to acknowledge funding from the British Heart Foundation grant PG/07/107/23895.

REFERENCES

Allard L, Soulez G, Chayer B, Treyve F, Qin Z, Cloutier G. Multimodality vascular imaging phantoms: A new material for the fabrication of realistic 3-D vessel geometries. Med Phys 2009;36:3758–3763.

Beattie DK, Golledge J, Cuming R, Greenhalgh RM, Davies AH. Duplex imaging and renal artery stenosis. J Vasc Investig 1997;3:52–60.

Brewin MP, Pike LC, Rowland DE, Birch MJ. The acoustic properties, centered on 20 MHz, of an IEC agar-based tissue-mimicking material and its temperature, frequency and age dependence. Ultrasound Med Biol 2008;34:1292–1306.

Browne JE, Ramnarine KV, Watson AJ, Hoskins PR. Assessment of the acoustic properties of common tissue-mimicking test phantoms. Ultrasound Med Biol 2003;29:1053–1060.

Dabrowski W, Dunmore-Buyze J, Cardinal HN, Fenster A. A real vessel phantom for flow imaging: 3-D Doppler ultrasound of steady flow. Ultrasound Med Biol 2001;27:135–141.

Dabrowski W, Dunmore-Buyze J, Rankin RN, Holdsworth DW, Fenster A. A real vessel phantom for imaging experimentation. Med Phys 1997;24:687–693.

Daigle RJ, Stravos AT, Lee RM. Overestimation of velocity and frequency values by multi element linear arrays Doppler. J Vasc Technol 1990;14:206–213.

Douville Y, Johnston KW, Kassam M, Zuech P, Cobbold RS, Jares A. An *in vitro* model and its application for the study of carotid Doppler spectral broadening. Ultrasound Med Biol 1983;9:347–356.

Frayne R, Gowman LM, Rickey DW, Holdsworth DW, Picot PA, Drangova M, Chu KC, Caldwell CB, Fenster A, Rutt BK. A geometrically accurate vascular phantom for comparative studies of x-ray, ultrasound, and magnetic resonance vascular imaging: construction and geometrical verification. Med Phys 1993;20:415–425.

Goldstein A, Langrill LN. Ethylene glycol-water mixture for use in ultrasound test objects. J Clin Ultrasound 1979;7:465–470.

Grant EG, Benson CB, Moneta GL, Alexandrov AV, Baker JD, Bluth EI, Carroll BA, Eliasziw M, Gocke J, Hertzberg BS, Katarick S, Needleman L, Pellerito J, Polak JF, Rholl KS, Wooster DL, Zierler E. Carotid artery stenosis: Grayscale and Doppler ultrasound diagnosis–society of radiologists in ultrasound consensus conference. Ultrasound Q 2003;19:190–198.

Hoskins PR. Velocity estimation using duplex scanners. Ultrasound Med Biol 1991;17:195–199.

Hoskins PR. Accuracy of maximum velocity estimates made using Doppler ultrasound systems. Br J Radiol 1996;69:172–177.

Hoskins PR. Simulation and validation of arterial ultrasound imaging and blood flow. Ultrasound Med Biol 2008;34:693–717.

IPEM Report No. 70. York: IPEM; 1994.

King DM. Development of renal phantoms for the evaluation of current and emerging ultrasound techniques, PhD dissertation 2009; Dublin Institute of Technology, Dublin.

Law YF, Johnston KW, Routh HF, Cobbold RS. On the design and evaluation of a steady flow model for Doppler ultrasound studies. Ultrasound Med Biol 1989;15:505–516.

Meagher S, Poepping TL, Ramnarine KV, Black RA, Hoskins PR. Anatomical flow phantoms of the nonplanar carotid bifurcation, part II: Experimental validation with Doppler ultrasound. Ultrasound Med Biol 2007;33:303–310.

Netuka D, Benes V, Mandys V, Hlasenska J, Burkert J, Benes V Jr. Accuracy of angiography and Doppler ultrasonography in the detection of carotid stenosis: A histopathological study of 123 cases. Acta Neurochir (Wien) 2006;148:511–520.

O'Flynn PM, Roche ET, Pandit AS. Generating an *ex vivo* vascular model. ASIAIO J 2005;51:426–433.

Olin JW, Piedmonte MR, Young JR, DeAnna S, Grubb M, Childs MB. The utility of Duplex ultrasound scanning of the renal arteries for diagnosing significant renal artery stenosis. Ann Intern Med 1995;122:833–838.

Paven G, Waugh R, Nicholson J, Gillin A, Hennessy A. Screening tests for renal artery stenosis: A case-series from an Australian tertiary referral centre. Nephrology (Carlton.) 2006;11:68–72.

Poepping TL, Nikolov HN, Rankin RN, Lee M, Holdsworth DW. An *in vitro* system for Doppler ultrasound flow studies in the stenosed carotid artery bifurcation. Ultrasound Med Biol 2002;28:495–506.

Poepping TL, Nikolov HN, Thorne ML, Holdsworth DW. A thin-walled carotid vessel phantom for Doppler ultrasound flow studies. Ultrasound Med Biol 2004;30:1067–1078.

Radermacher J, Brunkhorst R. Diagnosis and treatment of renovascular stenosis–a cost-benefit analysis. Nephrol Dial Transplant 1998;13: 2761–2767.

Ramnarine KV, Anderson T, Hoskins PR. Construction and geometric stability of physiological flow rate wall-less stenosis phantoms. Ultrasound Med Biol 2001;27:245–250.

Ramnarine KV, Nassiri DK, Hoskins PR, Lubbers J. Validation of a new blood-mimicking fluid for use in Doppler flow test objects. Ultrasound Med Biol 1998;24:451–459.

Renaudin CP, Barbier B, Roriz R, Revel D, Amiel M. Coronary arteries: New design for three-dimensional arterial phantoms. Radiology 1994;190:579–582.

Rickey DW, Picot PA, Christopher DA, Fenster A. A wall-less vessel phantom for Doppler ultrasound studies. Ultrasound Med Biol 1995;21:1163–1176.

Smith RF, Rutt BK, Holdsworth DW. Anthropomorphic carotid bifurcation phantom for MRI applications. J Magn Reson Imaging 1999;10: 533–544.

Staub D, Canevascini R, Huegli RW, Aschwanden M, Thalhammer C, Imfeld S, Singer E, Jacob AL, Jaeger KA. Best duplex-sonographic criteria for the assessment of renal artery stenosis–correlation with intra- arterial pressure gradient. Ultraschall Med 2007;28: 45–51.

Teirlinck CJ, Bezemer RA, Kollmann C, Lubbers J, Hoskins PR, Ramnarine KV, Fish P, Fredeldt KE, Schaarschmidt UG. Development of an example flow test object and comparison of five of these test objects, constructed in various laboratories. Ultrasonics 1998;36: 653–660.

Watts DM, Sutcliffe CJ, Morgan RH, Meagher S, Wardlaw J, Connell M, Bastin ME, Marshall I, Ramnarine KV, Hoskins PR, Black RA. Anatomical flow phantoms of the nonplanar carotid bifurcation, part I: Computer-aided design and fabrication. Ultrasound Med Biol 2007;33:296–302.

Wilhjelm JE, Vogt K, Jespersen SK, Sillesen H. Influence of tissue preservation methods on arterial geometry and echogenicity. Ultrasound Med Biol 1997;23:1071–1082.

Williams GJ, Macaskill P, Chan SF, Karplus TE, Yung W, Hodson EM, Craig JC. Comparative accuracy of renal duplex sonographic parameters in the diagnosis of renal artery stenosis: paired and unpaired analysis. AJR Am J Roentgenol 2007;188:798–811.

Yedavalli RV, Loth F, Yardimci A, Pritchard WF, Oshinski JN, Sadler L, Charbel F, Alperin N. Construction of a physical model of the human carotid artery based upon *in-vivo* magnetic resonance images. J Biomech Eng 2001;123:372–376.